J. Fluid Mech. (2010), *vol.* 661, *pp.* 178–205.
doi:10.1017/S0022112010002892

Streamwise vortices in shear flows: harbingers of transition and the skeleton of coherent structures

PHILIP HALL[1]† AND SPENCER SHERWIN[2]

[1]Institute of Mathematical Sciences, Imperial College London, London SW7 2AZ, UK

[2]Department of Aeronautics, Imperial College London, London SW7 2AZ, UK

(Received 13 August 2009; revised 17 May 2010; accepted 18 May 2010;
first published online 16 August 2010)

The relationship between asymptotic descriptions of vortex–wave interactions and more recent work on 'exact coherent structures' is investigated. In recent years immense interest has been focused on so-called self-sustained processes in turbulent shear flows where the importance of waves interacting with streamwise vortex flows has been elucidated in a number of papers. In this paper, it is shown that the so-called 'lower branch' state which has been shown to play a crucial role in these self-sustained processes is a finite Reynolds number analogue of a Rayleigh vortex–wave interaction with scales appropriately modified from those for external flows to Couette flow, the flow of interest here. Remarkable agreement between the asymptotic theory and numerical solutions of the Navier–Stokes equations is found even down to relatively small Reynolds numbers, thereby suggesting the possible importance of vortex–wave interaction theory in turbulent shear flows. The relevance of the work to more general shear flows is also discussed.

Key words: control theory, nonlinear instability, transition to turbulence

1. Introduction

Our concern is with the relationship between stationary streamwise vortex structures and wave systems in shear flows. The secondary instability of streamwise vortex flows is now well-understood and the agreement found between theory and experiment for vortices is arguably one of the successes of boundary-layer stability theory. It has been known since Davey, DiPrima & Stuart (1968) that a stationary Taylor vortex at finite amplitude suffers a secondary bifurcation to wavy vortex flows. Elsewhere, notably in discussions of shear-layer instabilities, the wavy vortex is referred to as the sinuous mode of instability, and often a second mode called the varicose mode can exist. The varicose mode has the primary and secondary instability in phase in the spanwise direction so that cell boundaries are no longer wavy.

In the context of the Görtler vortex problem, Hall & Horseman (1991) found that both modes are possible in external flows over curved walls but that in the configuration appropriate to the experiments of Swearingen & Blackwelder (1987) the sinuous mode dominates. Yu & Liu (1991) carried out a related calculation where the viscous terms in the instability equations were arbitrarily retained, their conclusions were broadly in agreement with Hall & Horseman (1991). Li & Malik (1995) subsequently gave a much more exhaustive discussion of the different secondary

† Email address for correspondence: philhall@ic.ac.uk

instability routes and also showed that in some cases the varicose mode can be unstable and also found that subharmonic modes can be unstable.

There are many other flows which support stationary vortex structures. In some circumstances, the vortices are produced directly by a centrifugal or buoyancy instability, see for example Hall & Morris (1992), or as a result of imperfections, e.g. wall roughness, though in the absence of a secondary instability these vortices would ultimately decay to zero. Our work is relevant to all of these situations but for definiteness we will concentrate on a much simpler problem namely Couette flow between rigid walls.

In the absence of curvature or heating or any other direct mechanism to produce streamwise vortices, the unperturbed flow is often stable to inviscid waves. However, one can imagine a situation where a wave is sufficiently large to produce a driving mechanism for streamwise vortices which themselves are unstable to waves. Such a self-sustaining configuration was the subject of several papers some years ago; see for example Hall & Smith (1988, 1989, 1990, 1991), Bassom & Hall (1989), Bennett, Hall & Smith (1991), Blackaby (1991) and Walton & Smith (1992). In these papers the wave system was described asymptotically and was either a Tollmien–Schlichting or an inviscid wave. For obvious reasons this type of interaction was referred to as a vortex–wave interaction.

It is convenient to introduce some more recent terminology for streamwise vortex flows. Consider a flow $(u(y), 0, 0)$ which is modified by some means to produce a velocity field $\boldsymbol{u}(y, z)$ which is periodic in the spanwise z direction. We refer to the flow associated with the y–z velocity components as a streamwise 'roll' and the downstream velocity component u corresponds to what is called a 'streak'. The combination of the streamwise rolls and downstream streaks then make a streamwise vortex. An examination of the Navier–Stokes equations at large values of the Reynolds number R shows that an exact Navier–Stokes solution is possible with the rolls of size R^{-1} and the streaks $O(1)$. This scaling can be traced back to the work of for example Taylor (1923) on small gap Taylor vortices. If there is curvature associated with the flow then the y momentum equation is driven by a centrifugal term proportional to u^2 whilst the streak is driven directly by the rolls through nonlinearity.

The key observation made in the Hall–Smith theory was that the required forcing of the vortex system could be achieved by tiny waves because wave interactions preferentially drive the rolls which themselves drive the streaks. In fact, both inviscid and viscous waves can drive the latter rolls which are of size R^{-1} so that the flow $\boldsymbol{u}$, which we refer to as the streamwise vortex, can be driven by small waves. The vortex–wave interaction theories therefore describe nonlinear states where an $O(1)$ streak is driven by a wave field that satisfies a linear eigenvalue partial differential equation with coefficients which depend on the streak which is itself driven by a roll forced by the wave field. In spatially developing or temporally varying mean states, the wave field adjusts locally or instantaneously so as to remain neutral during the evolution process. The theory failed however to shed a great deal of light on the transition process where small linear waves amplify through various stages until they become highly nonlinear, though some work on the relevance of the theory to the initiation process was given by Hall (1994) and Brown *et al.* (1993). What we demonstrate in this paper is that the theory is in all likelihood much more directly relevant to turbulent flows and indeed that the theory gives remarkably good agreement with recent large direct numerical computations of coherent states in shear flows.

Some years before the work of Hall & Smith (1991), a mechanism somewhat related to vortex–wave interaction theory had been postulated by Benney (1984).

However, in that theory the Reynolds number was $O(1)$ and there was no rational way to asymptotically deduce an interaction mechanism. Essentially, Benney wrote down reduced forms of the Navier–Stokes equations which could be used as a starting process to derive the vortex–wave interaction theories by using the limit of large Reynolds numbers. It was also not recognized that the interaction can only take place if the wave system remains neutral during the interaction. Apart from Hall & Smith (1991), the waves were taken to be Tollmien–Schlichting waves induced by viscosity, and a generic property was found to be that their forcing of the vortex occurs in a viscous boundary layer with the asymptotic structure of the wave described by triple-deck theory. Later Chapman (2002) considered subcritical instabilities of channel flows by looking at the linear instability of uniform flows perturbed by spanwise periodic structures. Chapman isolated the size of spanwise periodic perturbation in the y, z planes which could destabilize Couette flow and found it to be $O(R^{-1})$. This is entirely consistent with the vortex–wave interaction theories which have the fundamental structure of an $O(1)$ streaky flow driven by an $O(R^{-1})$ roll. However, in Chapman's work the instability of the streaky flow is so small that it has no back effect on the rolls and the spanwise periodic flow leading to instability is imposed on the flow. Thus, Chapman's work only overlaps with the vortex–wave interaction theory work in the isolation of the size of rolls which drive a streaky flow which can be unstable.

Most of the vortex–wave interaction work has been in the context of viscous waves but in Hall & Smith (1991) the interaction equations were also given for a flow supporting inviscid waves of the type found by Hall & Horseman (1991). It was found that the forcing takes place in the critical layer associated with the wave and drives a discontinuity in the roll shear and pressure. No solutions of the full interaction system found by Hall & Smith (1991) have yet been published. The solution of these equations is the primary concern of this paper.

More recently still there has been immense interest in nonlinear processes in shear flows and their relationship with coherent structures which occur in turbulent flows. These processes have come to be known as 'self-sustained processes' and are typified by wave systems driving rolls which themselves drive streaks which are themselves neutrally stable to the wave. This process sounds very much like the one identified in the vortex–wave interaction work. This apparent connection between self-sustained processes and vortex–wave interaction theories has not been explored. Here we will show the relationship between the two approaches in the context of channel flows but there exists many closely related results for pipe flow (see for example Hof *et al.* 2004; Fitzgerald 2004; Wedin & Kerswell 2004; Kerswell & Tutty 2007; Viswanath 2007; Faisst & Eckhardt 2003).

In channel flows, Waleffe and co-workers, guided by the early ideas of Benney and co-workers, in a number of papers looked into the possibility that the Navier–Stokes equations might support wave systems occurring as instabilities of streamwise vortex flows with the waves sufficiently large to drive the vortex flows (see for example Waleffe 1995, 1997, 1998, 2001, 2003; Wang, Gibson & Waleffe 2007). The approach used was to find fully nonlinear solutions of the Navier–Stokes equations using fictitious body forces to find equilibrium states and then continue them when the forcing was switched off. Earlier, Nagata (1990) had done related calculations with the nonlinear flow initially driven by centrifugal effects and then connected them to a finite amplitude state as the Taylor number was decreased to zero. Much greater detail of these structures was revealed subsequently in for example the paper by Clever & Busse (1997).

Of particular relevance to this paper, and indeed the major motivation for it, is the work reported in a numerical investigation of Couette flow by Wang *et al.* (2007). That paper was concerned with self-sustained interactions in Couette flow over a range of Reynolds numbers. The equilibrium solutions found were computed by first driving a vortex flow using a fictitious body force in the spanwise momentum equation. In the calculations, finite amplitude solutions were found above some Reynolds numbers with the solutions then connecting to what the authors referred to as upper and lower branch states. (Note that this choice of label, though understandable since the upper and lower branches correspond to flows with higher and lower drags respectively, is different from the usual convention of shear flow instability theory where the lower and upper branches of the neutral curve correspond to viscous and inviscid modes, respectively, whereas we will show that the lower branch modes are in fact inviscid.) Particular interest was given to the lower branch states and the authors found that the calculations could be resolved even at high Reynolds numbers with minimal Fourier modes in the streamwise direction. These equilibrium states were found by Newton iteration and not by marching the equations of motion forward in time. Numerically, they observed that the vortex was forced by the wave in a critical layer where the wave speed coincided with the downstream velocity, in fact that velocity was zero so the waves were stationary. The lower branch states discussed by Wang *et al.* (2007) corresponded to waves which were in fact stationary which happens because of the symmetries of Couette flow driven by boundaries moving in equal and opposite directions.

The lower branch states have been shown in a number of papers to play a crucial role in determining whether a flow is going to become turbulent or return to the laminar state. For example, following the suggestion made by Waleffe (2003), Schneider *et al.* (2008) talk about the 'edge' as being the surface separating initial states which develop into turbulence and those which relaminarize and they show conclusively that the edge can be associated directly with the lower branch states. Obviously, an asymptotic theory such as ours which can reveal the structure of the edge will be invaluable to those undertaking large-scale computations and indeed open the door to possible turbulent flow manipulations by a suitable modification of the possible wavelengths and stability properties of the streaks.

The above picture of the lower branch state associated with Couette flow is exactly the scenario of the Hall & Smith (1991) theory, though the latter was of course formulated in the context of boundary layers. In addition, Wang *et al.* (2007) suggested from their numerical results that the wave amplitude of the spanwise velocity component should scale like $R^{-0.9}$ whilst the streak and rolls scale like R^0 and R^{-1}, respectively. We will show that our approach gives excellent agreement with the numerical work of Wang *et al.* (2007) over a wide range of Reynolds numbers. In computational terms, we see that the vortex–wave interaction theory reduces the computational problem from a three-dimensional unsteady Navier–Stokes calculation to a two-dimensional steady Navier–Stokes problem at unit Reynolds number coupled to a linear wave evolution equation.

The original formulation of the vortex–wave interaction equations given by Hall & Smith (1991) was derived in Cartesian coordinates and will be modified here to give the interaction equations for Couette flow. We note that the equations in Cartesian form appear to break down when the critical layer is locally vertical. Though that situation does not apply to Couette flow, it certainly would be the case for circular Poiseuille flow. In what follows we have formulated a relatively straightforward and accessible derivation of the interaction equations for arbitrary geometry which

overcomes this difficulty and indeed highlights the key physical processes acting in vortex–wave interactions/self-sustained processes.

Our alternative approach uses ideas from steady streaming theory; see for example Stuart (1966) and Riley (1967). The key idea is that an inviscid wave propagating on a streaky flow has a critical layer of depth $R^{-1/3}$ centred on the position where the wave speed and streak velocity coincide. Since the streaky flow varies in the z direction then the critical layer position in the spanwise direction varies. As the critical layer is approached, the wave amplitude increases so the maximum wave motion takes place in this layer. Moreover, in this layer the wave velocity components in the plane perpendicular to the streaky flow are bigger than the roll velocity. The time periodic motion in the layer generates a mean motion independent of time and the downstream coordinate in the same way as oscillatory boundary layers generate steady streaming. Unlike the latter case the wave stresses cause a jump in the roll shear and pressure across the layer, thereby driving the rolls. In fact, the jump in roll pressure is induced to balance a centripetal acceleration of the wave due to the streaming motion whilst the jump in the roll shear is induced by the mean stresses parallel to the critical layer. Thus, the physical process at the heart of vortex–wave interactions, or indeed self-sustained processes, is a steady streaming effect leading to a jump in the roll shear and local centrifugal pressure gradient of the rolls.

In the next section we present a relatively straightforward alternative derivation of the interaction equations for Couette or indeed any flow in a channel of arbitrary cross-section. As part of the derivation we will describe the key features of the partial differential equation governing the inviscid wave system. A discussion of the numerical method used to solve the interaction equations follows in § 3, together with a discussion of the results obtained in § 4. Finally, we end by drawing some conclusions from this investigation.

2. Vortex–wave interactions in Couette flow

The starting point is the non-dimensional momentum and continuity equations for an unsteady viscous fluid of constant density. Following the usual notation these may be taken in the form as

$$\widetilde{\boldsymbol{u}}_t + \widetilde{\boldsymbol{u}} \cdot \nabla \widetilde{\boldsymbol{u}} = -\nabla \widetilde{p} + \frac{1}{R} \nabla^2 \widetilde{\boldsymbol{u}}, \tag{2.1}$$

$$\nabla \cdot \widetilde{\boldsymbol{u}} = 0. \tag{2.2}$$

Here $\widetilde{p}$ is the kinematic pressure and R is a suitably scaled Reynolds number; for example for Couette flow the Reynolds number is based on the maximum Couette flow velocity and the channel half-height. We will be interested in the limit of this parameter tending to infinity. If we are concerned with flow between parallel plates moving in opposite directions then the above equations are to be solved subject to

$$\widetilde{\boldsymbol{u}} = (\pm 1, 0, 0), \quad y = \pm 1, \tag{2.3}$$

so that Couette flow $u = [y, 0, 0]$ is a possible solution. For channels of arbitrary cross-section a unidirectional flow is still possible with $u = u(y, z)$ and u satisfying the no-slip condition at the boundary.

2.1. *Vortex system*

Equations (2.1)–(2.2) allow an exact Navier–Stokes solution of the form

$$\widetilde{\boldsymbol{u}} = [u(y, z, T), v(y, z, T)/R, w(y, z, T)/R], \quad p = -Gx/R + p(y, z, T)/R^2, \tag{2.4}$$

which has velocity field independent of x and where $T = t/R$ is a slow diffusion time chosen to balance convection and viscous diffusion. The constant term in the pressure has been inserted to cover the case when the unidirectional base state is driven by the motion of the walls and a pressure gradient. The relative scalings of the velocity components are the usual ones for centrifugal instabilities in the small gap, or thin boundary-layer limit, and were first identified by Taylor (1923). The equations of motion then reduce to

$$u_T + vu_y + wu_z = G + u_{yy} + u_{zz}, \tag{2.5}$$

$$v_T + vv_y + wv_z + p_y = v_{yy} + v_{zz}, \tag{2.6}$$

$$w_T + vw_y + ww_z + p_z = w_{yy} + w_{zz}, \tag{2.7}$$

$$v_y + w_z = 0, \tag{2.8}$$

subject to the same boundary conditions. We see that the y and z momentum equations (2.6) and (2.7) decouple from the streamwise momentum equation (2.5). So if the y and z equations are solved for v, w then the x momentum equation can be independently solved for the u component leading to the streaks. If curvature is present and appropriately scaled then the above equations reduce to the full nonlinear equations for Taylor vortices in the small gap limit when a term T_0u^2 is inserted into the y momentum equation. However, in the absence of any forcing we might expect that the appropriate solution of the roll equations is simply $v = w = p = 0$ since the effective Reynolds number is now unity and the unperturbed zero state is certainly stable. Thus, we expect that in the absence of forcing, any perturbation of the roll-streak flow away from Couette flow would ultimately decay to zero.

2.2. *Wave system*

Suppose that we now take the Reynolds number to be large and assume we have a steady roll/streak flow described by the above equations and we superimpose on it a wave periodic in the x direction with wavenumber α. The time scale for the evolution of the streamwise vortex flow corresponds to T whereas an inviscid wave will evolve on the faster time scale RT. Therefore, we look for a wave with instantaneous frequency $\Omega = \alpha Rc(T)$. The wave will be described by the inviscid analysis of streaks given by Hall & Horseman (1991) and when the wave speed $c(T)$ is real, it will have a critical layer $y = f(z)$ where $u = c$.

Away from the critical layer we write

$$\tilde{u} = u(y, z, T) + \cdots + \delta R^{-1/3}(\rho(T)U(y, z, T)E + \text{c.c.}) + \cdots, \tag{2.9}$$

$$\tilde{v} = R^{-1}v(y, z, T) + \cdots + \delta R^{-1/3}(\rho(T)V(y, z, T)E + \text{c.c.}) + \cdots, \tag{2.10}$$

$$\tilde{w} = R^{-1}w(y, z, T) + \cdots + \delta R^{-1/3}(\rho(T)W(y, z, T)E + \text{c.c.}) + \cdots, \tag{2.11}$$

$$\tilde{p} = -R^{-1}Gx + R^{-2}p(y, z, T) + \cdots + \delta R^{-1/3}(\rho(T)P(y, z, T)E + \text{c.c.}) + \cdots, \tag{2.12}$$

where c.c. denotes complex conjugate. In the above it has been assumed that, since the wave depends on length scales of the same size in each direction, the velocity components of the wave must be of similar magnitude, and $\rho(T)$ is the slowly varying wave amplitude. The relative size of the pressure is then fixed from the balance $u(\partial U/\partial x) \sim (\partial P/\partial x)$ and the size of the wave $\delta R^{-1/3}$ will be fixed within the critical layer where it becomes $O(\delta)$. The quantity E appearing above is

defined by

$$E = \exp\left(\mathrm{i}\alpha\left[x - R\int^{T} c(T)\,\mathrm{d}T\right]\right). \tag{2.13}$$

If we substitute the expansions (2.9)–(2.12) into the Navier–Stokes equations (2.1) and (2.2) and look at the leading-order terms of order R^{-1} and R^{-2}, independent of E, we see that u, v, w, p satisfy (2.5)–(2.8). Similarly, the leading-order terms of size $\delta R^{-1/3}$ and proportional to ρE satisfy the inviscid linearized Navier–Stokes equations:

$$\mathrm{i}\alpha(u-c)U + Vu_y + Wu_z = -\mathrm{i}\alpha P, \tag{2.14}$$

$$\mathrm{i}\alpha(u-c)V = -P_y, \tag{2.15}$$

$$\mathrm{i}\alpha(u-c)W = -P_z, \tag{2.16}$$

$$\mathrm{i}\alpha U + V_y + W_z = 0. \tag{2.17}$$

If we follow Hall & Horseman (1991) and eliminate U, V and W from the above equations then we see that P satisfies

$$P_{yy} + P_{zz} - \alpha^2 P - \frac{2u_y P_y}{u-c} - \frac{2u_z P_z}{u-c} = 0. \tag{2.18}$$

This equation must be solved subject to the normal derivative of P vanishing at any rigid boundary and periodicity in the spanwise direction. This equation is the generalization into two dimensions of the pressure form of Rayleigh equation which governs the linear instability of a unidirectional flow depending on a single variable. No general results have yet been proved for this equation. We know from Hall & Horseman (1991) and Li & Malik (1995) that, in the case when the downstream velocity field corresponds to a Görtler vortex of spanwise wavelength Λ, both synchronous and subharmonic eigenmodes with wavelengths Λ and 2Λ respectively are possible, though invariably the synchronous modes are the most unstable. Of the synchronous modes, the wavy one, sometimes referred to as sinuous mode, is usually the most unstable and it is this mode that causes the onset of wavy vortices in the Taylor vortex problem. For a given spanwise wavenumber α and streak velocity field $u(y, z, T)$, we have an eigenvalue problem for the complex wave speed $c(T)$. We are interested in equilibrium solutions where the waves do not grow (or decay) on the RT timescale, and so we must stipulate that c is purely real. Note that if this is not the case then the interaction of the waves we will consider shortly would cause the vortex to grow (or decay) exponentially in time at twice the rate as the waves. For a given streak velocity there will therefore be only a finite number of pairs $(\alpha, c(T))$ which are acceptable.

2.3. *Interaction in the critical layer*

If we prescribe the real wavenumber α, the streak velocity field must adjust as T varies in order to make it possible to compute a corresponding real eigenvalue $c(T)$. Furthermore, (2.14)–(2.17), or equivalently (2.18), will then have a critical layer at $y = f(z, T)$, where the streak velocity satisfies $u(y, z, T) = c$. In this layer viscous effects smooth out any singularities and the layer is then of the usual thickness $R^{-1/3}$. Note however that it may be possible to use nonlinear effects to smooth out the singularity but that needs a reconsideration of the size of the roll and might also be the origin of the upper branch modes.

It follows from (2.14)–(2.16) that as the critical layer is approached, U, V, W all behave like $(y - f)^{-1}$. A further discussion of the critical layer can be found in

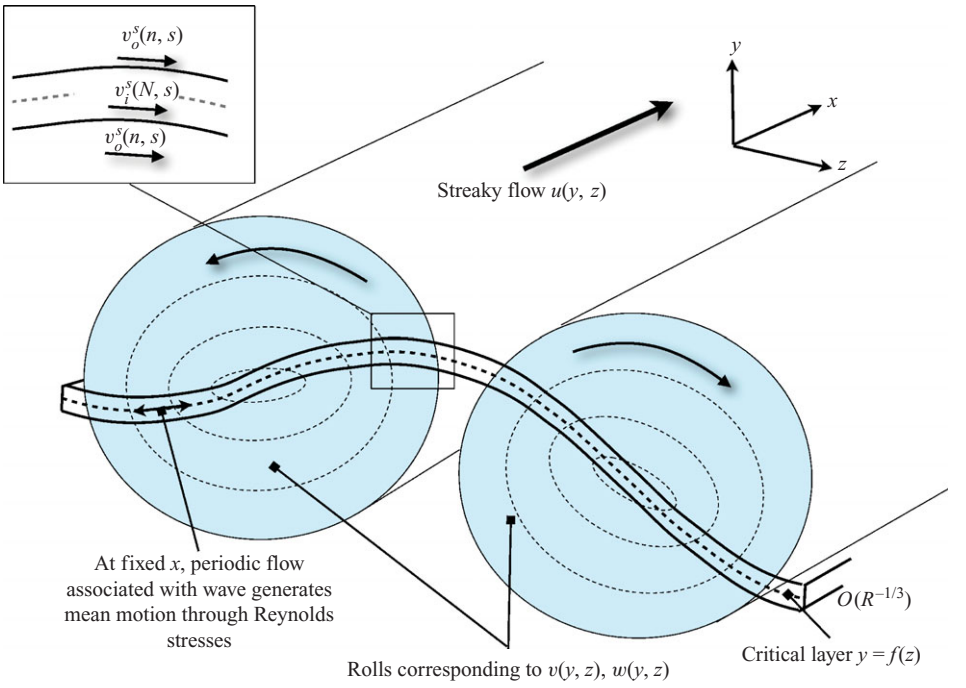

FIGURE 1. (Colour online) Sketch of critical layer intersecting rolls. Note that the location of layer varies with z and the Reynolds stresses associated with wave trapped in the critical layer generate a mean motion leading to jumps in the roll normal shear and pressure across critical layer with all other components of shear and velocity continuous.

Blackaby & Hall (1994) and Timoshin & Smith (1997) but the main point to note is that as the critical layer is approached, P is regular and remains $O(1)$. In different situations it appears that there can be a logarithmic singularity at higher order in the neutral case but, as pointed out by Timoshin & Smith (1997), the vortex–wave interaction equations of Hall & Smith (1991) are independent of whether or not such a singularity occurs at higher order.

In order to find a relatively straightforward derivation of the interaction equations between the wave and vortex systems in the critical layer, we diverge from the approach of Hall & Smith (1991) and use local coordinates (x, n, s) with n, s measuring distance normal and tangential to the critical layer at a fixed x. At such a fixed value of x, the wave leads to a time-periodic sloshing motion concentrated within the critical layer which is centred on $y = f(z)$; see figure 1.

The Reynolds stresses associated with this motion vary in s and so will produce a steady streaming. It is this steady streaming which, in a rather novel way, produces the forcing of the rolls needed to sustain the interaction between the waves and the streamwise vortex. If we define a critical layer variable $N = R^{1/3}n$, then with respect to the x, N, s coordinate frame, the leading-order wave velocity in the critical layer is

$$\rho\delta(\mathscr{U}(N, s, T), R^{-1/3}\mathscr{V}(N, s, T), \mathscr{W}(N, s, T))E + \text{c.c.}, \tag{2.19}$$

whilst the pressure is

$$\rho\delta R^{-1/3}\mathscr{P}(N, s, T)E + \text{c.c.} \tag{2.20}$$

The wave amplitude φ is a function of T and remains arbitrary at this order since (2.18) is linear. Note that δ, the wave amplitude in the critical layer, is still to be determined. This is achieved by forcing the wave to drive a spanwise-periodic flow matching onto the roll solution outside the critical layer. If we denote the component of the roll velocity field (v, w) resolved in the s direction within the critical layer by $v_i^s(N, s, T)$ then the leading-order approximations to the s momentum equations is

$$\frac{1}{R^2}R^{2/3}\frac{\partial^2 v_i^s}{\partial N^2} = \delta^2\rho^2(-\mathrm{i}\alpha\mathscr{U}\overline{\mathscr{W}} + \mathscr{V}\overline{\mathscr{W}}_N + \mathscr{W}\overline{\mathscr{W}}_s) + \text{c.c.} + \cdots. \tag{2.21}$$

Here an overline denotes 'complex conjugate'. We recall that in steady streaming problems where an oscillatory flow interacts with a boundary, the corresponding equation when integrated shows that the streaming velocity, essentially v_i^s, does not decay to zero at infinity so an outer steady flow is generated. In the current problem, because the Reynolds stresses are acting in an internal layer, the situation changes slightly and integrating (2.21) once across the critical layer shows that the normal derivative of the tangential component of the roll velocity, v_i^s, across the critical layer has a jump which must be accommodated by the roll velocity field in the bulk of the flow.

Likewise, we write down the normal momentum equation as

$$\frac{1}{R^2}R^{1/3}\frac{\partial p^s}{\partial N} = -\delta^2\rho^2\Lambda_0(s, T)\mathscr{W}\overline{\mathscr{W}} + \text{c.c.} + \cdots, \tag{2.22}$$

where $\Lambda_0(s, T)$ is the local curvature of the critical layer and p^s the roll pressure in the critical layer parameterized in terms of arclength. If we integrate once across the layer, we find that there is a jump in the pressure. Note that the direction of the jump in pressure changes when the sign of the curvature of the critical layer changes.

Using the equation of continuity for the wave and noting that $\lim_{N\to\pm\infty}\mathscr{W} = 0$, it follows then that the normal derivative of the tangential component of the roll velocity and pressure for the flow external to the critical layer must satisfy:

$$\left[\frac{\partial v_o^s(n, s, T)}{\partial n}\right]_-^+ = 2\delta^2\rho^2R^{5/3}\int_{-\infty}^{\infty}\frac{\partial}{\partial s}|\mathscr{W}(N, s, T)|^2\,\mathrm{d}N, \tag{2.23}$$

and

$$[p]_-^+ = -2\Lambda_0\delta^2\rho^2R^{5/3}\int_{-\infty}^{\infty}|\mathscr{W}(N, s, T)|^2\,\mathrm{d}N. \tag{2.24}$$

Note that $v_o^s(n, s, T) = \boldsymbol{e}_s\cdot[0, v(y, z, T), w(y, z, T)]$ where $\boldsymbol{e}_s$ is a unit vector tangential to the critical layer. Hence, we see that by choosing $\delta = R^{-5/6}$ the outer equations for the roll velocity must be solved subject to a jump in the pressure and normal shear across the critical layer $y = f(z, T)$. We therefore deduce that the Hall & Smith (1991) theory leads to an asymptotic result which for Couette flow has the streak and roll velocities scaling like R^0, R^{-1} respectively, whilst the maximum size of the wave is $R^{-5/6}$ which occurs in the critical layer. Though this is reasonably close to the exponent 0.9 suggested by Wang *et al.* (2007), it turns out that the norm used by those authors is a little special and that, when we use the corresponding norm in our approach, the exponent increases to 11/12, in remarkable agreement with Wang *et al.* (2007).

The structure given above for the rolls, streaks and wave pressure field and jump conditions applies to channels of arbitrary cross-section. Though in this paper we are interested in Couette flow, the extension to more general cross-sections is achieved by merely specifying the new boundary shape on which the no-slip condition is to be applied. In particular, the structure applies to circular Poiseuille flow so that it is

possible that many of the structures found in turbulent pipe flows owe their origins to the vortex–wave interaction theory. If that is indeed the case, then the vortex–wave interaction theory for inviscid waves holds the key to the understanding of one of the fundamental structures of turbulent shear flows and it raises the possibility that this knowledge might profitably be used to tune some turbulent flow properties such as drag by the preferred excitation of particular vortex wavelengths; see also Wang *et al.* (2007) for a discussion of this possibility.

The jump conditions (2.23) and (2.24) found above apply to vortex–wave interactions in a channel of arbitrary cross-section and are simplified further by writing down the form for $\mathscr{W}(n, s)$. From the momentum equation in the s direction for the wave in the critical layer, it is found that at leading order $\mathscr{W}(n, s, T)$ satisfies

$$\frac{\partial^2 \mathscr{W}(N, s, T)}{\partial N^2} - \mathrm{i}\alpha\mu(s, T) N \mathscr{W}(N, s, T) = \frac{\partial \mathscr{P}(N, s, T)}{\partial s}, \tag{2.25}$$

whilst the N-component momentum equation gives

$$\frac{\partial \mathscr{P}(N, s, T)}{\partial N} = 0. \tag{2.26}$$

Here $\mu(s, T) = (\partial u/\partial n)(f(s), z(s), T)$ is the normal derivative of the streak $u(y, z, T)$ evaluated on the critical layer and therefore is a function of s, T only. The second equation implies that the wave pressure in the critical layer is independent of N, and therefore matching with the wave outside the critical layer we deduce that

$$\mathscr{P}(N, s, T) = P(y = f(z(s), T), z(s), T). \tag{2.27}$$

The equation for $\mathscr{W}$ is to be solved such that it decays to zero at $\pm\infty$. The solution of this equation can be expressed in terms of Scorer functions and, after some manipulation, we find that

$$\mathscr{W} = -(\alpha\mu)^{-2/3} \frac{\partial \mathscr{P}(s, T)}{\partial s} \int_0^\infty \exp(-\mathrm{i}(\alpha\mu)^{1/3}(Nk - k^3/3)\, \mathrm{d}k. \tag{2.28}$$

Using the above equations we can then show that the jump equations reduce to

$$\left[\frac{\partial V^s(n, s, T)}{\partial n}\right]_-^+ = n_0 \rho^2 \alpha^{-5/3} \frac{\partial}{\partial s}\left(\mu^{-5/3} \left|\frac{\partial \mathscr{P}}{\partial s}\right|^2\right), \tag{2.29}$$

and

$$[p]_-^+ = -n_0 \rho^2 (\alpha\mu)^{-5/3} \Lambda_0 \left|\frac{\partial \mathscr{P}}{\partial s}\right|^2, \tag{2.30}$$

where $n_0 = 2\pi(2/3)^{2/3}(-2/3)$. We are now in a position to summarize the effect of the wave on the roll which we recall satisfies (2.6)–(2.8). Firstly, note that these equations are to be solved subject to the no-slip conditions at any boundary. At the critical layer $y = f(z, T)$, the velocity components v, w are continuous but the normal derivative of the roll velocity tangential to the critical layer and the pressure must satisfy the jump condition. The jump conditions are functions of the pressure eigenfunction $P(y, z, T)$ evaluated on the critical layer. Having determined the roll velocity, the streak velocity follows from (2.5) which is to be solved subject to no slip at any boundary and with u and its derivatives continuous across the critical layer. The pressure eigenfunction P must then satisfy (2.18) and this equation then closes the system for the roll, streak and wave velocity. At first sight the pressure equation looks linear but in fact u depends on P through u, v so the equation is nonlinear. If we assume all quantities

are known at an instant T then the equations must be stepped forward in time in such a way that the new pressure satisfies (2.18) at the new time step and $c(T)$ must remain real, this is achieved by suitably varying the amplitude function $\rho(T)$. We now wish to apply this general formulation to Couette flow. For computational purposes it is convenient to restate the jump conditions in Cartesian form. If we define

$$\Delta = 1 + f_z^2, \tag{2.31}$$

$$a = \lambda\alpha/\Delta, \tag{2.32}$$

where $\lambda = u_y(f, z, T)$, then the conditions become

$$[w_y]_-^+ = \frac{[v_y]_-^+}{f_z} = J(z, T), \tag{2.33}$$

$$J = \frac{n_0}{a^{5/3}\Delta^5}\rho^2 \left\{ \left(-\frac{7\Delta_z}{2\Delta} - \frac{5a_z}{3a} \right) \left| \frac{\partial P}{\partial z} \right|^2 + \frac{\partial}{\partial z}\left(\left| \frac{\partial P}{\partial z} \right|^2 \right) \right\}, \tag{2.34}$$

$$[p]_-^+ = K = -\frac{n_0}{a^{5/3}\Delta^5}\rho^2 f_{zz} \left| \frac{\partial P}{\partial z} \right|^2, \tag{2.35}$$

where $\pm$ signs denote values evaluated above and below the critical layer and all z derivatives are to be evaluated along the critical layer $y = f(z)$, i.e.

$$\left. \frac{\partial}{\partial z} \right|_{y=f(z)} = \left. \frac{\partial}{\partial z} \right|_y + f_z \left. \frac{\partial}{\partial y} \right|_z . \tag{2.36}$$

The above forms are the same as derived by Hall & Smith (1991) but we note that the simplification of the current formulation was found by working with coordinates along and normal to the critical layer. Finally, note that $\mathscr{P}$ in (2.29) and (2.30) is simply P parameterized in terms of the arclength.

We are now in a position to summarize the interaction equations. Firstly, the vortex and pressure fields $\boldsymbol{u}$, p satisfy (2.5)–(2.8) and must be solved subject to periodicity in the spanwise direction and the no-slip boundary conditions at any rigid boundary. In addition, at the critical level $y = f(z, T)$, the velocity $\boldsymbol{u}$ is continuous whilst v_y, w_y, p satisfy the jump conditions (2.33)–(2.35), and these jump conditions are a function of the wave pressure, which satisfies (2.18), evaluated on the critical layer.

2.4. *Comparison with the results of Wang et al. (2007)*

We now demonstrate how the scaling results of Wang *et al.* (2007) for the wave part of the velocity field can be obtained from the asymptotic structure given above. To make this comparison, we must determine M_w, the maximum in y of the root mean square (r.m.s.) in the spanwise direction of the spanwise component of the wave. The key point here is that the wave is largest within the critical layer. In view of our scalings above, the wave part of this quantity is of size $R^{-7/6}$ outside the critical layer and of size $R^{-5/6}$ in the critical layer. At a fixed y we can compute the contributions to the integral in the definition of the r.m.s. by evaluating the contributions within and outside the critical layer. If the critical layer is not horizontal at the given value of y, the contributions to the integral from outside and inside the critical layer give terms of size $R^{-7/3}$ and $R^{-5/3}R^{-1/3}$, respectively, so the dominant contribution comes from the critical layer and the r.m.s. will be of size R^{-1}. However, at a value of y where $f_z = 0$ the critical layer will extend a distance $R^{-1/6}$ in the spanwise direction so the contribution to the integral of the square of the modulus of the wave amplitude

will now be like $R^{-11/6}$ so that the maximum in the wall-normal direction of the r.m.s. in z will occur where the critical layer is locally horizontal and will be of size $R^{-11/12}$.

Thus, the maximum in y of the spanwise component of the wave will occur at some value of the critical layer variable $Y = R^{1/3}(y - f)$. At any value of Y, we can write the spanwise component of the wave down using (2.28) and we then evaluate numerically the value of Y where the maximum in Y of the r.m.s. in z of the spanwise component of the wave velocity occurred. If we write

$$\Phi_0 = \frac{2^{1/4}\,|P_z|}{a^{3/4}\Lambda^{1/2}\Delta^2\,|f_{zz}|^{1/4}} \tag{2.37}$$

and evaluate this at a point where $f_z = 0$, then we find that this maximum value M_w is

$$M_w = 2.268\rho\Phi_0 R^{-11/12}. \tag{2.38}$$

2.5. *Regularization of the wave interactions on the roll velocity*

In the next section, we will concentrate on finding equilibrium solutions of the interaction equations and so we drop all the T dependence in the vortex momentum equations and take

$$E = \exp(\mathrm{i}\alpha[x - cRT]). \tag{2.39}$$

The major computational challenge is the solution of the y, z nonlinear momentum equations (2.6) and (2.7) for the vortex. If we assume J and K are known then we require the solution of the two-dimensional steady Navier–Stokes equations at unit Reynolds number in the y,z plane subject to no slip at $y = \pm 1$ and periodicity in the z direction. Of course, the periodicity is fixed by the forcing associated with the jump conditions (2.33)–(2.35). In what follows we will solve these equations using a spectral element discretization due to Karniadakis & Sherwin (2005). Rather than building the jump conditions into the scheme, it is convenient to regularize the equations to take care of the jump in a more conventional setting for this type of discretization. In order to do so, we introduce forcing functions into the momentum equations such that the equations of motion become

$$vv_y + wv_z = -p_y + v_{yy} + v_{zz} + F_1, \tag{2.40}$$

$$vw_y + ww_z = -p_z + w_{yy} + w_{zz} + F_2, \tag{2.41}$$

$$v_y + w_z = 0. \tag{2.42}$$

We then choose functions $F_1(y, z)$ and $F_2(y, z)$ to automatically enforce the required jumps at the critical layer. Next, we suppose the forcing functions in (2.40) and (2.41) take the form

$$F_1 = f_1(z)\delta\,(u - c)\,, \tag{2.43}$$

$$F_2 = f_2(z)\delta\,(u - c)\,, \tag{2.44}$$

where we have assumed that the wave speed is purely real. We first note that

$$\int_{f_-}^{f_+} F_1(u - c)\,\mathrm{d}y = \int_{f_-}^{f_+} \frac{1}{\lambda} f_1 \delta(u - c)\,\mathrm{d}u = \frac{1}{\lambda} f_1, \tag{2.45}$$

where we have used the previous definition $\lambda = u_y(f, z, T)$. For quantities that jump over the critical layer, the derivative normal to the critical layer is much larger than

any derivative tangential to the layer. We can also argue that

$$\left.\frac{\partial}{\partial z}\right|_{y=f(z)} \simeq -f_z \left.\frac{\partial}{\partial y}\right|_z \tag{2.46}$$

so if we evaluate the y-integral of (2.40) across the critical layer and use (2.33), we observe that

$$0 = -K + f_z J + f_z^3 J + \frac{1}{\lambda} f_1(z), \tag{2.47}$$

and so

$$f_1 = \lambda \left[K - \Delta f_z J\right], \tag{2.48}$$

where Δ is defined in (2.31). Likewise, the z momentum equation (2.41) produces

$$0 = f_z K + J + f_z^2 J + \frac{1}{\lambda} f_2(z), \tag{2.49}$$

so that

$$f_2 = -\lambda \left[f_z K + \Delta J\right]. \tag{2.50}$$

In other words, if the functions f_1, f_2 are chosen as indicated in expressions (2.48) and (2.50), then the solution of the regularized equations will automatically produce the required jumps at the interface and the delta function can then be defined in terms of the limiting form of a smooth function. In our calculations we approximate the Dirac delta function as

$$\widetilde{\delta}_\chi(\varphi) = \frac{\exp(-\varphi^2/\chi)}{\sqrt[2]{\chi\pi}}. \tag{2.51}$$

We confine our calculations to the case of plane Couette flow so the pressure gradient G is henceforth taken to be zero. In the absence of a wave or vortex, the basic state, plane Couette flow, is antisymmetric about $y=0$, so there is no preferred direction for a wave to move and we might expect a solution of the vortex–wave interaction problem to exist with $c=0$. Of course solutions pairs propagating to the right and left with equal and opposite wave speeds might exist but we do not look for them here. Having regularized the two-dimensional Navier–Stokes equations, the streamwise momentum equation can be solved with no discontinuities in u or its first-order derivatives. Having found u, the eigenvalue problem associated with the wave pressure equation can be solved. In the following section a detailed discussion of the numerical scheme we adopt is provided but before doing so it is instructive to make a few observations about the symmetries of the problem under consideration. All of our calculations concern waves having the same spanwise periodicity as the vortex state though it should be remembered that subharmonic modes are possible; see Li & Malik (1995). The underlying vortex field has the symmetry

$$u(y, z) = -u(-y, z + \Lambda/2), \tag{2.52}$$

$$v(y, z) = -v(-y, z + \Lambda/2), \tag{2.53}$$

$$w(y, z) = w(-y, z + \Lambda/2), \tag{2.54}$$

where Λ is the spanwise wavelength of the vortex field. This symmetry means that if the wave equation when $c_r = 0$ has a solution $P(y, z)$ then we can choose the solution such that for $z \geqslant 0$

$$P(y, z) = -\overline{P}(-y, z + \Lambda/2). \tag{2.55}$$

Note that solutions not having this property can exist but we concentrate on solutions having this property. In fact, if we choose the origin such that u is an even function of z then the pressure field can be either odd or even in z but, as first found in Hall & Horseman (1991), the odd mode seems the preferred one so that

$$P(y, z) = \overline{P}(-y, -z + \pi/\gamma). \tag{2.56}$$

The equation for P is of course linear so the solution must be normalized, and so we choose to normalize P such that

$$\sqrt{\frac{\int |P|^2 \, \mathrm{d}A}{A}} = 1. \tag{2.57}$$

3. A numerical scheme for the solution of the interaction equations

We outline an iterative process to determine the solution of the interaction equations. We start by giving a brief overview of our iterative scheme and subsequently discuss each part of the iteration in more detail. We stress that our numerical procedure is designed specifically to determine equilibrium solutions of the vortex–wave interaction equations for Couette flow. Thus, our aim is to see whether the asymptotic structure we have provided in § 2 captures the equilibrium lower branch states of Wang *et al.* (2007) found from the full Navier–Stokes equations. Note once again that the latter authors sought equilibrium solutions directly from the Navier–Stokes equations and then studied their instability as a secondary instability problem. They found that the lower branch states had a single unstable eigenvalue which approached zero approximately like $R^{-1/2}$. Since the time evolution appropriate to vortex–wave interactions is on a longer $O(R)$ time scale, it is not possible for our formulation to capture the secondary instability; we discuss this point further in our conclusions.

The first step is to be clear about exactly what is the nature of the nonlinear eigenvalue problem for equilibrium vortex–wave states. Suppose that we fix the spanwise wavenumber $\gamma = 2\pi/\Lambda$ of the roll-streak flow and α the wavenumber of the inviscid wave system driving the rolls. The interaction equations we have formulated might then be expected to have solutions for some values of the parameters ρ, c_r where $c = c_r + \mathrm{i}0$. However, because of the symmetry of our problem, a solution is possible with $c_r = 0$ so for each γ and α there will, in principle, be a corresponding eigenvalue $\rho = \rho(\alpha, \gamma)$. Our scheme to find this eigenvalue is based on guessing a value for $\rho(\alpha, \gamma)$ and finding the corresponding complex eigenvalue $0 + \mathrm{i}c_i$ and then varying ρ until we drive c_i to zero.

Suppose then that at step k of our iteration procedure we have a streak velocity field u^k. Using this field we can find a solution of the pressure equation (2.18), and we will obtain the corresponding pressure P^k and eigenvalue $0 + \mathrm{i}c_i^k$. Having found the pressure field, we can compute the regularized jump terms in the roll equations and by marching them forward in time we compute the steady-state values of v^k, w^k. The streak equation is then solved directly for the new streak velocity u^{k+1}. The procedure is then continued until convergence is achieved. More formally, then for fixed α, $\gamma = 2\pi/\Lambda$, and ρ we undertake the following steps.

(i) Using $u^k(y, z)$ as a base flow, solve the pressure equation to obtain $P^k(y, z)$. In fact, as we explain in more detail later, instead of solving the pressure equation we solve the linearized Navier–Stokes equations governing the instability of the streak.

These equations will contain a pseudo-Reynolds number $\widetilde{R}$. In the limit when $\widetilde{R}$ tends to infinity, this pressure field becomes the required solution of (2.18). At this step we also obtain the leading imaginary temporal eigenvalue $0 + \mathrm{i}c_i^k$.

(ii) Using u^k and P^k from step (i), normalized according to (2.57), evaluate the regularized forcing

$$\widetilde{F}_1^k(z) = f_1(u^k(z), P^k(z))\widetilde{\delta}_\chi(u^k), \tag{3.1}$$

$$\widetilde{F}_2^k(z) = f_2(u^k(z), P^k(z))\widetilde{\delta}_\chi(u^k). \tag{3.2}$$

(iii) Now substitute for the regularized forcing from step (ii) into the roll equations for v^k, w^k. In these equations we retain the time derivatives and obtain the steady-state solutions by marching them forward in time.

(iv) Finally, using the roll solution v^k, w^k from step (iii), solve a steady-state advection–diffusion system for the x-component streak momentum u^{k+1}, as will be detailed shortly (see (3.16)). At this point, the mesh can be restructured to align with the new critical layer at $u(y, z) = 0$.

The symmetries of the interaction problem are numerically imposed on $\widetilde{F}_1^{k+1}(z)$, $\widetilde{F}_2^{k+1}$ in step (iii) and the cycle is iterated until $|c_{im}^k - c_{im}^{k-1}| < \epsilon$, where ϵ is the tolerance. A series of iterations is then performed for a range of values of ρ at fixed α, γ until we can determine the required value of ρ at the given values of α, γ by interpolating the (ρ, c_i) data to find the point at which $c_i = 0$. Alternatively, at step (i) we have also investigated a sub-iteration to adjust α until $c_i \simeq 0$. This was also implemented in conjunction with varying the value of ρ in step (iii) so that the search was restricted to a fixed line in the (ρ, α) space. We observed that searching along the line $\rho^2 = \alpha^{5/3} + \text{const}$ or $\rho = C_1\alpha + \text{const}$ (for $0.7 \leqslant C_1 \leqslant 0.8$) allowed us to more efficiently obtain the equilibrium solution when $\alpha > 0.3$. Finally, we note that two numerical parameters are required in each iterative cycle, $\widetilde{R}$ and χ, and we will demonstrate the sensitivity to these parameters later.

We note that in step (iii) we solve a time-dependent two-dimensional Navier–Stokes problem, whereas in step (iv) we solve the steady-state equation directly for the roll. The solutions for $u(y, z)$, $v(y, z)$, $w(y, z)$ obtained in steps (iii) and (iv) are therefore not solutions of the unsteady Navier–Stokes problem which corresponds to the retention of the time derivative in all three momentum equations. This approach therefore has the benefit that our partly unsteady scheme is not capturing the time-dependent evolution of an equilibrium state which based on the work of Waleffe (2003) appears to be unstable and therefore could not be captured by marching the full unsteady problem forward in time. Finally, we note that so long as the solution eventually settles and becomes steady, we have an equilibrium state of the interaction equations but the solution procedure along the way is not a solution of the full unsteady problem which requires the time dependence in the streamwise momentum equation to be enforced and ρ to be taken as a function of time in order to keep $c_i = 0$ as required in the unsteady interaction equations. Also, we note that the steady-state solution achieved is only acceptable in the derivation of the interaction equations if $c_i = 0$ and this is achieved by carrying out runs with different amplitudes ρ.

All of the steps in the iterative scheme are solved using a spectral/hp element discretization; see Karniadakis & Sherwin (2005) for more details. This type of discretization can use an elemental decomposition into either triangular or quadrilateral subdomains as shown in figure 2(a). In this mesh, we have chosen to capture the region around the critical layer $u(f, z) = 0$ within a quadrilateral layer of elements to help resolve the steep regularized forcing $\widetilde{F}_{1,2}^k(z)$ which contains the

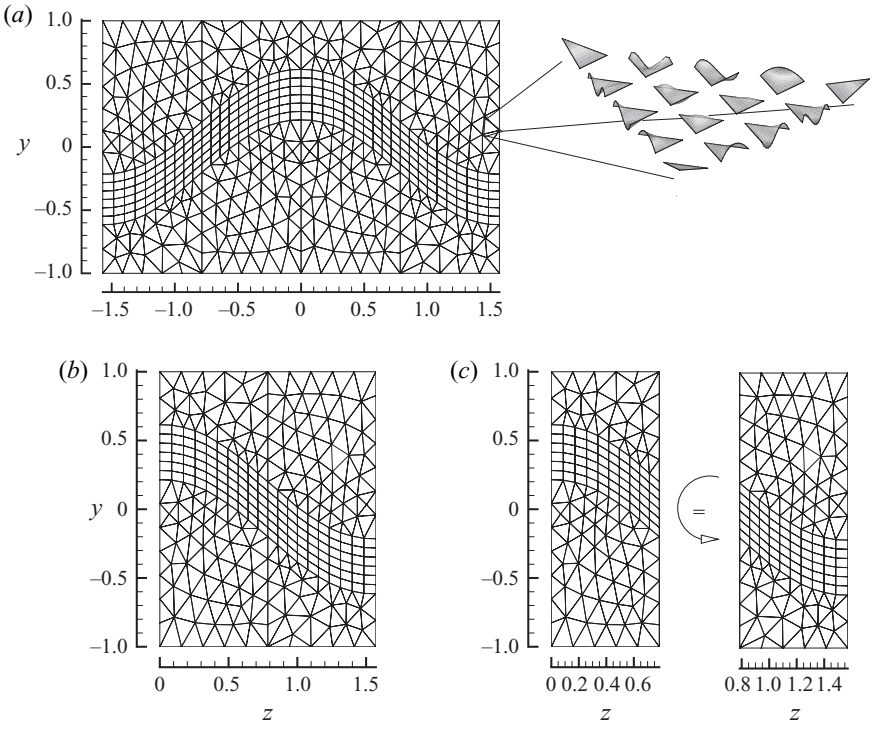

FIGURE 2. Figure of computational domain: (*a*) elemental discretization of full equivalent computational domain and an illustration of expansion modes used in each triangular region for a fourth-order polynomial approximation; (*b*) half computational domain adopted in simulations; (*c*) rotational quarter symmetry of computational domain.

approximation to a Dirac delta function. To ensure that the regularized forcing is adequately captured, we can uniformly increase the resolution within each element by increasing the polynomial approximation used within each subdomain as indicated on the right of figure 2(*a*), where we observe the polynomial modes used within a single triangular subdomain for a fourth-order approximation.

Finally, since the critical layer is not fixed in the z direction due to the periodicity of the interaction problem, we 'pin' the location of the layer by solving in a half-domain as indicated in figure 2(*b*) and imposing boundary conditions to be specified shortly. In addition, we have also designed our half-mesh to have a further level of symmetry about the quarter length in z as indicated in figure 2(*c*). This rotational similarity of the quarter domain allows us to enforce the desired symmetries on $\widetilde{F}_{1,2}(z)$ and indirectly on the whole interaction problem. This enforcement of symmetry has been numerically observed to be necessary to ensure we obtain eigenvalues c which have zero real part. In the following, we discuss each of these iterative steps in more details.

3.1. *Step (i): P from the linearized Navier–Stokes equations*

Rather than solving the generalized inviscid Rayleigh equation (2.18) directly, we obtain the wave solution $P(y, z)\exp(\mathrm{i}\alpha x)$ as the largest eigenvalue of the inverse of the linearized Navier–Stokes equations about the base flow state $\boldsymbol{u}(y, z) = [u(y, z), 0, 0]$.

If the viscous terms in these linearized equations are neglected, we recover the inviscid perturbation equations (2.14)–(2.18). The viscous equations are then solved at

higher and higher values of the Reynolds number, $\widetilde{R}$, until the results are independent of the Reynolds number. Note that the solution of the pressure equation (2.18) given by Hall & Horseman (1991) does not apply to the non-neutral case, and to extend that approach we would have to make a detour in the integration path in the y direction into the complex plane using the usual procedure. In order to do so, the streak velocity would need to be extended into the complex plane which would be computationally expensive, so we choose to calculate the pressure eigenfunction as the limiting form of a high-Reynolds-number eigenvalue problem. To obtain the largest eigenvalue of the inverse of the linearized Navier–Stokes problem, we use an Arnoldi iteration where the inner iteration requires the inversion of the operator $\mathscr{L}(\boldsymbol{u})$ as

$$\mathscr{L}\begin{bmatrix}\boldsymbol{U}\\ P\end{bmatrix} = \begin{bmatrix}-\frac{1}{\widetilde{R}}\nabla^2 + \boldsymbol{u}\cdot\nabla + (\nabla\boldsymbol{u})^{\mathrm{T}} & \nabla\\ -\nabla\cdot & 0\end{bmatrix}\begin{bmatrix}\boldsymbol{U}\\ P\end{bmatrix} \tag{3.3}$$

subject to the boundary conditions. It would also be possible to solve this problem in the full domain shown in figure 2(a) with periodic spanwise boundary conditions:

$$U(\pm 1, z) = V(\pm 1, z) = W(\pm 1, z) = 0, \tag{3.4}$$

$$U(y, 0) = V(y, 0) = \frac{\partial W}{\partial z}(y, 0) = 0, \tag{3.5}$$

$$U(y, \Lambda/2) = V(y, \Lambda/2) = \frac{\partial W}{\partial z}(y, \Lambda/2) = 0. \tag{3.6}$$

To discretize $\mathscr{L}$ we again apply the spectral hp element method this time with a $P_{N+1} - P_{N-1}$ domain deocomponsition technique as discussed by LeTallec & Patra (1997) and Ainsworth & Sherwin (1999). We note that the pressure is normalized to satisfy condition (2.57) and the value of the pseudo Reynolds number is taken to be fixed value (typically $\widetilde{R} = 1000$) for $\alpha > 0.9$ and $\widetilde{R} = 1000/\alpha$ for $\alpha < 0.9$.

In earlier studies, we also solved this problem by obtaining the leading eigenvalue of the linearized Navier–Stokes equations using a time-marching technique as the inner part of the Arnoldi iteration (Tuckerman & Barkley 2000; Barkley, Blackburn & Sherwin 2008). This approach gave consistent answers but required a significantly longer time to obtain the relevant eigenvalue.

3.2. *Step (ii): critical-layer forcing*

In the next step we have to evaluate the regularized forces for the v, w momentum equations, which are defined as

$$\widetilde{F}_1(y, z) = f_1(z)\widetilde{\delta}_\chi(u) = \lambda\,[K - \Delta f_z J]\,\frac{\exp(-u^2/\chi)}{\sqrt{\pi\chi}}, \tag{3.7}$$

$$\widetilde{F}_2(y, z) = f_2(z)\widetilde{\delta}_\chi(u) = -\lambda\,[f_z K + \Delta J]\,\frac{\exp(-u^2/\chi)}{\sqrt{\pi\chi}}, \tag{3.8}$$

where Δ, a, J and K are as defined in (2.31)–(2.35) and $\lambda = u_y(f, z)$.

We note that $u(y, z)$ and $P(y, z)$ and their partial derivatives can be evaluated everywhere in the y, z plane, although in the limit of $\chi \to 0$ only their values on the interface are important. Note also that f_z, f_{zz} can be expressed in terms of first- and second-order derivatives of u. We are now able to evaluate all terms arising in $f_1(z)$ and $f_2(z)$ as functions of y–z and then multiply these functions by $\widetilde{\delta}_\chi(u)$, which restricts the forcing function to a region around the critical layer whose thickness is dependent upon χ.

3.3. *Step (iii): v, w momentum equations*

The third step in our iterative cycle involves the solution of the steady state v, w vortex equations (2.6)–(2.8). However, to numerically handle the nonlinearity of the vortex system, we march the y–z equations

$$v_t^k + vv_y^k + wv_z^k + p_y^k = v_{yy}^k + v_{zz}^k + \widetilde{F}_1^k, \tag{3.9}$$

$$w_t^k + v^k w_y^k + w^k w_z^k + p_z^k = w_{yy}^k + w_{zz}^k + \widetilde{F}_2^k, \tag{3.10}$$

$$v_y^k + w_z^k = 0, \tag{3.11}$$

forward in time until an equilibrium state is achieved. At every time step, we impose zero Dirichlet conditions on the upper and lower wall and symmetry conditions on the two sides of the domains, i.e.

$$v^k(\pm 1, z) = w^k(\pm 1, z) = 0, \tag{3.12}$$

$$v_z^k(y, 0) = w^k(y, 0) = 0, \tag{3.13}$$

$$v_z^k(y, \Lambda/2) = w^k(y, \Lambda/2) = 0. \tag{3.14}$$

For initial conditions we either impose the solution from the previous cycle v^{k-1}, w^{k-1} or zero conditions on the first iteration $k = 0$. This step requires the solution of a two-dimensional forced Navier–Stokes problem which we time march using a second order in time accurate velocity correction scheme (Karniadakis, Israeli & Orszag 1991; Guermond & Shen 2003) based upon a spectral/hp element discretization. We recall that the above system has a unit Reynolds number. In our simulations we have observed that this viscous damping appears to be sufficient to stabilize the flow to reach a steady state.

3.4. *Step (iv): u momentum equation*

Having determined $v(y, z)$ and $w(y, z)$ we now solve the u momentum equation (2.5), which is essentially a forced advection–diffusion problem. Since the underlying driving component of u is Couette flow, we can decompose u into

$$u^k(y, z) = y + u'(y, z), \tag{3.15}$$

and recast (2.5) as

$$\frac{\partial^2 u'}{\partial y^2} + \frac{\partial^2 u'}{\partial z^2} - v\frac{\partial u'}{\partial y} - w\frac{\partial u'}{\partial z} = v, \tag{3.16}$$

subject to the boundary conditions

$$u'(\pm 1, z) = 0, \qquad u'_z(y, 0) = 0, \qquad u'_z(y, \Lambda/2) = 0. \tag{3.17}$$

Once again, this equation is approximated on the mesh shown in figure 2 using a Galerkin projection with a spectral/hp element spatial discretization.

3.5. *Numerical validation*

Before discussing the results in the following section, it is worth considering some validation of the numerical implementation and investigating the influence of the parameters we have chosen. In undertaking our study we consider a spanwise wavenumber of $\gamma = 2$ as shown in figure 2, which was also adopted in the study of Wang *et al.* (2007). Furthermore, unless stated otherwise in what follows, we fix the regularization parameter $\chi = 1/1000$ and the pseudo-Reynolds number in our stability calculations to $\widetilde{R} = 1000$.

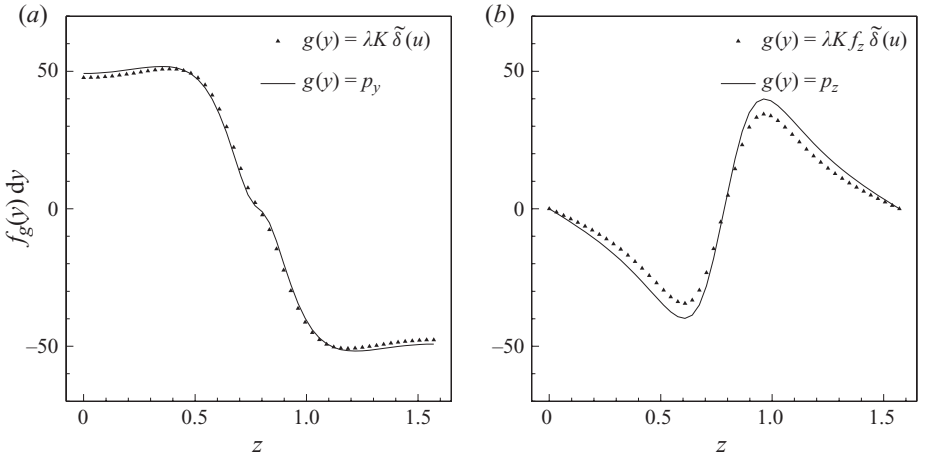

FIGURE 3. Comparison of the integral of (*a*) p_y, (*b*) p_z (solid lines) over the critical layer with jump conditions λK and $\lambda K f_z$, respectively (triangles).

Motivated by Waleffe (2003), we initiate our iteration with a two-dimensional divergence-free body forcing term of the form

$$\widetilde{F}_1(y, z) = C\gamma \cos(\pi y)\cos(\gamma z), \tag{3.18}$$

$$\widetilde{F}_2(y, z) = C\pi \sin(\pi y)\sin(\gamma z), \tag{3.19}$$

where $C = 20$. This artificial body force generates a roll solution and it can then be substituted into the streak equation which is then solved. This streak velocity is then used in step (i) of our procedure outlined above. However, note that having determined this initial streak the artificial body force is switched off and $\widetilde{F}_1(y, z)$, $\widetilde{F}_2(y, z)$ replaced by the jump forms of these quantities.

3.6. *Enforcement of the regularized forcing*

Starting with the streak computed as described above from the artificial forcing given in (3.18) and (3.19), we undertake a single iteration through steps (i)–(iv) and evaluate the regularized forcing $\widetilde{F}_1^1$, $\widetilde{F}_2^1$ from (3.1) and (3.2). We then time march the v, w momentum equations to a steady state using this updated regularized forcing as discussed in step (iii). At this point, we can ask how well the jump conditions (2.33) and (2.35) are enforced. All simulations were performed using eighth-order polynomial expansions within every elemental domain.

In order to check that our regularization procedure is working, we numerically evaluate the following integrals:

$$\int_{f-\epsilon}^{f+\epsilon} p_y \,\mathrm{d}y = \int K\, \widetilde{\delta}_\chi(u)\,\mathrm{d}u = \int_{f-\epsilon}^{f+\epsilon} \lambda K\, \widetilde{\delta}_\chi(u)\,\mathrm{d}y, \tag{3.20}$$

$$\int_{f-\epsilon}^{f+\epsilon} p_z \,\mathrm{d}y = \int K\, f_z\, \widetilde{\delta}_\chi(u)\,\mathrm{d}u = \int_{f-\epsilon}^{f+\epsilon} \lambda K\, f_z\, \widetilde{\delta}_\chi(u)\,\mathrm{d}y, \tag{3.21}$$

across the critical layer. At every z location we numerically determine the critical layer $y = f(z)$ using a Newton iteration with a tolerance of 1×10^{-8}. We then integrate over the interval $f - \epsilon < y < f + \epsilon$, where $\epsilon = 0.05$ using 31 Gauss–Lobatto–Legendre integration points. We observe from figure 3 that the two integrals balance relatively well for the finite approximation of the Dirac delta function using $\widetilde{\delta}_\chi(u)$

a		b	
$\widetilde{R}$	αc_i	χ	αc_i
1000	3.42×10^{-2}	1/1000	3.42×10^{-2}
2000	3.59×10^{-2}	1/2000	3.46×10^{-2}
5000	3.67×10^{-2}	1/5000	3.49×10^{-2}
10 000	3.69×10^{-2}		

TABLE 1. Variation of growth, αc_i, as a function of $\widetilde{R}$ and χ for $\alpha = 1$, $\gamma = 1$, $\rho = 1$.

with $\chi = 1/1000$. A balance containing all terms in the v, w momentum equations leads to an agreement to within the plotting error.

3.7. *Sensitivity of the eigenvalue growth rate to $\widetilde{R}$ and χ*

We next investigate the sensitivity of growth rate αc_i with respect to χ and $\widetilde{R}$. We consider the case of $\alpha = 1$, $\rho = 1$, $\gamma = 2$ and obtain the variation in the leading eigenvalue growth rate as shown in table 1. From this table we observe that the variation of growth is less than 3×10^{-3} when varying $\widetilde{R}$ from 1000 to 10 000 and is less than 1×10^{-3} if we vary χ from 1/1000 to 1/5000.

4. Results

In the first instance, we will discuss the results obtained for the particular configuration of Wang *et al.* (2007). As pointed out at the end of § 2 in Wang *et al.* (2007), the authors plotted the maximum in the wall-normal direction of the r.m.s. in the spanwise direction of the streak (with the contribution from Couette flow subtracted out), the spanwise component of the wave, and the rolls. Results were also given for higher harmonics but we do not calculate them in our theory.

Figure 4(*a*) shows a comparison of the corresponding quantities from our calculations. The dotted lines denote the predictions from our theory with the appropriate Reynolds number scalings applied. The agreement over a wide range of Reynolds numbers is remarkable, so there seems little doubt that our theory is describing the exact coherent structures found by Wang *et al.* (2007). In particular, the spanwise component of the wave conforms well to the non-integer scaling of $R^{-11/12}$ given by (2.38). Thus, exact coherent structures which are believed to have a strong relationship with coherent structures observed in turbulent shear flows are produced by an inviscid instability of a streak interacting with itself to drive a roll which then modifies the original streak and so on. Figure 4(*b*) should be compared with figure 2(*g*) of Wang *et al.* (2007). We observe that there is good agreement between the asymptotic theory and the full numerical calculations of the latter authors. The vortex wave approach to the identification of exact coherent structures has the advantage that the Reynolds number is taken out of the problem and that solutions for a wide parameter range can be readily computed. Now that we have convincing evidence that vortex–wave interaction theory and the lower branch states are one and the same thing, it is interesting to look at other parameter ranges and give results which would be prohibitively expensive to compute directly from the Navier–Stokes equations.

Following the procedure outlined in § 3, we consider the results for the case with $\gamma = 2$, where we have fixed $\chi = 1/1000$, and will define $\widetilde{R} = 1000$ shortly. In figure 5, we plot the line of zero growth $\alpha c_i = 0$ as a function ρ, α where we have considered the range $0.1 \leqslant \alpha < 1.5$. For the given spanwise number, the plot therefore shows the relationship between the wave amplitude and wavenumber needed to drive a

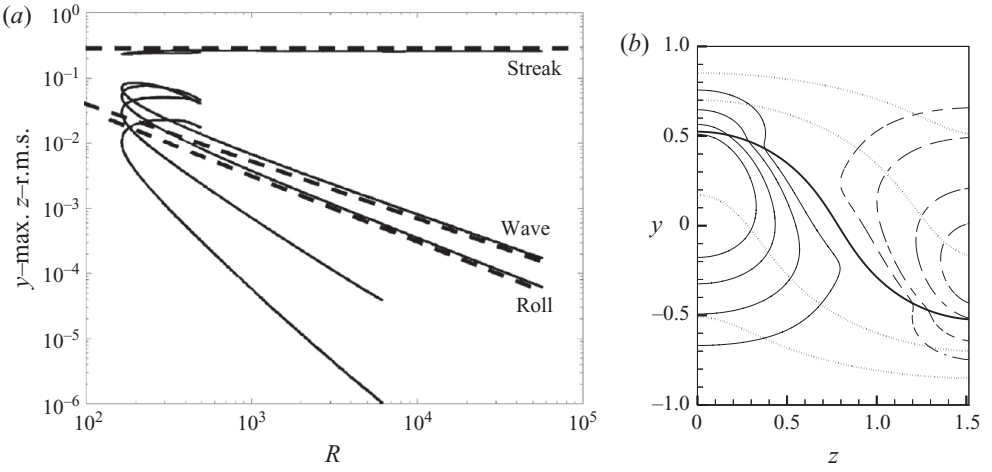

FIGURE 4. (*a*) Comparison of amplitudes of direct numerical simulations of Wang *et al.* (2007) (solid lines) with the current theory (dashed lines). The top almost coincident and horizontal curves corresponds to the maximum in y of the r.m.s. in z of the streak velocity with Couette flow subtracted out, i.e. $u(y,z)-y$. The curves labelled wave and roll correspond to the same quantities evaluated for the spanwise wave velocity component and the roll velocity. (*b*) Comparison with figure 2 (top) of Wang *et al.* (2007) at $(\alpha,\gamma)=(1.213,2)$, dotted lines denote streak flow, solid and dashed lines denote positive and negative vertical roll velocity and the bold solid curve highlights the critical layer.

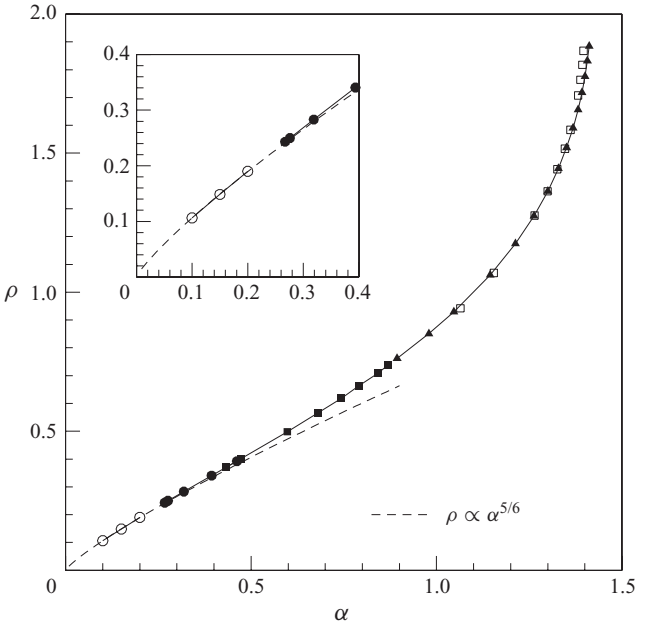

FIGURE 5. Data of ρ versus α at a zero growth rate is achieved in the nonlinear iterations of §3. Also shown by a dashed line is the plot of $\rho=C\alpha^{5/6}$, where the constant C is fixed by the data at $\alpha=0.05$. Symbols correspond to different iteration strategies as detailed in the text.

streak neutrally stable to the wave. Interestingly, the solution approaches the origin at small wavenumbers which means long-wave instabilities are possible and indeed their asymptotic structure can be readily identified. Note, however, that at sufficiently

small wavenumbers, viscous effects will contribute at leading order to the evolution of the wave and the theory will fail when the wavenumber varies like some inverse power of the Reynolds number.

To obtain the data in figure 5, we ran exploratory cycles, for different values of ρ and a fixed value of α, of the steps outlined in § 3 until a fixed growth rate of the maximum eigenvalue of the inverse linearized Navier–Stokes problem was achieved. Having obtained values of ρ which span the region of neutral growth, we then refined the value of ρ through interpolation until we obtained a growth rate where $\alpha c_i \leqslant 1 \times 10^{-4}$. As discussed in § 3, we were then able to adopt a line search for other neutral points where we perform a sub-iteration to find the value of α where the growth rate is zero for a given critical layer. We have applied different line searches as denoted by the different symbols in this plot. The filled triangles correspond to searches along the lines $\rho = k\alpha^{5/6}$ (where k is a constant) with a psuedo-Reynolds number of $\widetilde{R} = 1000$. The open squares correspond to searches along the lines $\rho = k\alpha^{5/6}$ but with a psuedo-Reynolds number of $\widetilde{R} = 5000$. We note that at higher α values when the critical layer becomes steeper, the change in Reynolds number does have a small effect on the neutral curve. The closed squares correspond to searches along the lines $\rho = 0.7\alpha + k$, and the closed circles correspond to searches along the lines of $\rho = 0.75\alpha + k$ (where again k is a constant varied for each point in the neutral curve). Both of these sets of points used a psuedo-Reynolds number of $\widetilde{R} = 1000/\alpha$. Finally, the open circles correspond to a manual search at a fixed value of α and a pseudo-Reynolds number of $\widetilde{R} = 1000/\alpha$. For these last points, we were unable to find an automated search.

In the inset of figure 5 we show an enlargement of the neutral curve around the origin. In both plots we have indicated by a dashed line a fit of the form $\rho = C\alpha^{5/6}$ where the constant was fixed by the computed values at $\alpha = 0.1$. We observe that for a wide range of the smaller values of the wavenumber, the data agree well with this fit which is consistent with the scaling to make the value of the jump conditions (2.34) and (2.35) finite as $\alpha \to 0$. Indeed, the small α asymptotic structure can be readily identified by a consideration of the jump conditions (2.29) and (2.30), where we see that the balance $\rho = C\alpha^{5/6}$ at small wavenumbers keeps the right-hand sides $O(1)$ so that the roll driven by the jump conditions remains $O(1)$. Hence, in the small wavenumber limit, the roll and streak equations remain the same but the jump conditions have the combination $\rho^2\alpha^{-5/3}$ combined into a single $O(1)$ parameter. Finally, the pressure equation is then to be solved with the wavenumber α set equal to zero. Thus, in the limit of zero wavenumber, the streak does not collapse back into Couette flow. We stress here that the $\rho = C\alpha^{5/6}$ balance at small wavenumbers gives us the long wavelength limit of the interaction problem within the vortex–wave framework. When the wavenumber reaches some inverse power of the Reynolds number, viscous effects will come back into play and modify the small wavenumber structure. That calculation is beyond the scope of the present work. However, it is because of this effect that when we perform calculations at smaller and smaller values of α we must increase the pseudo-Reynolds number in order to capture the inviscid structure.

It turns out that there are different possibilities which exist for higher α that can be inferred from an asymptotic study of the interaction equations. Firstly, if a solution exists for large α, then the vertical concentration of the wave must shrink to a thickness $1/\alpha$ in which case we can show that $\rho = C_2\alpha^{11/6} + \cdots$. An obvious alternative scenario is for the solutions to have the wavenumber approaching a finite value with the wave amplitude tending to infinity. Finally, it could well be that the

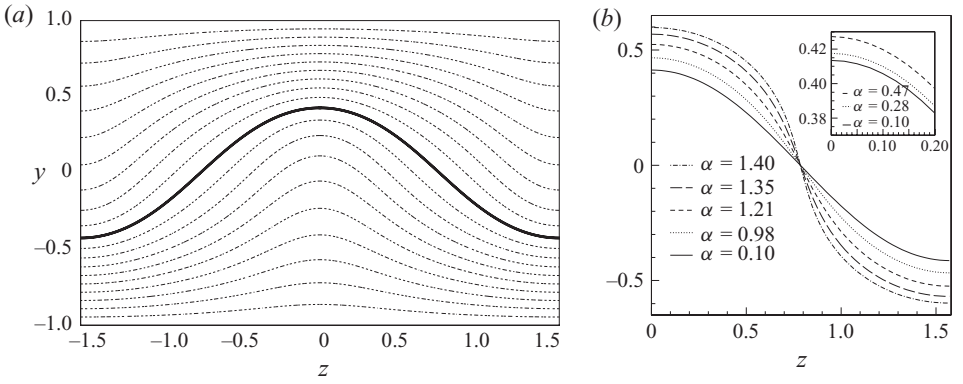

FIGURE 6. (*a*) Equispaced contours of $u(y, z)$ at $\alpha = 0.47$, $\gamma = 2$ and $\rho = \sqrt{0.161}$. The solid line highlights the location of the critical layer $u(y, z) = 0$. (*b*) Variation of the critical layer location in half the spanwise domain for $\gamma = 2$, $\alpha = 0.1, 0.98, 1.21, 1.35$ and 1.4. The inset shows the variation of the upper part of the critical layer at $\alpha = 0.1, 0.28$ and 0.47.

curve simply turns round and then enters the origin, though extensive searches near the origin only found a single branch of solutions. However, the results shown in figure 5 suggest that the wave amplitude goes to infinity as α approaches a finite value. Our calculations did not converge for values of the wavenumeber higher than those shown and we found no trace of a second branch of solutions shown above but we cannot be sure that the curve does not turn round.

In figure 6(*a*) we plot the values of the streak contours $u(y, z)$ for the case $\alpha = 0.47$, $\gamma = 2$, $\rho = \sqrt{0.161}$, where the growth rate was $\alpha c_i = -4.67 \times 10^{-5}$. The solid line in this plot indicates the critical layer where $u(y, z) = 0$ and all other contours are plotted at equispaced levels of 0.1. The deformation of the streamlines is typical of streaks associated with centrifugal instabilities, though the self-interaction of the wave is driving the vortex field. Once again, the contours shown agree well with results given by Wang *et al.* (2007). The shape of the contours does not vary significantly as the wavenumber is varied.

In figure 6(*b*) we highlight the variation of the critical layer in the region $0 \leqslant z \leqslant \pi/2$ for $\alpha = 0.1, 0.98, 1.21, 1.35$ and 1.4 at the neutral condition of zero growth where the corresponding values of ρ are given in figure 5. The inset indicates an enlargement of the interface variation for $0 \leqslant z \leqslant 0.15$, where we have also indicated the location of the critical layer at $\alpha = 0.1, 0.28$ and 0.47. We observe that for lower values of $\alpha < 0.5$ the interface is relatively constant. As we increase α further the interface appears to approach a limiting configuration. This suggests that the right-hand branch corresponds to a vertical asymptote rather than the other possibilities discussed earlier.

Figure 7 shows a variety of features of the wave solution. In this figure, we see the same results for three different neutral points corresponding to $\alpha = 0.2$, $\gamma = 2$, $\rho = \sqrt{0.035438}$ (figure 7*a*,*b*), $\alpha = 0.8$, $\gamma = 2$, $\rho = \sqrt{0.4405}$ (figure 7*c*,*d*) and $\alpha = 1.4$, $\gamma = 2$, $\rho = \sqrt{3.1537}$, $\widetilde{R} = 1000$ (figure 7*e*,*f*). In each of these series of plots we observe isocontours of the axial (figure 7*a*,*b*) and the spanwise (figure 7*e*,*f*) components of the wave velocity. Also indicated at the ends of the isocontours are the roll velocity and the critical layers. The other two-dimensional isocontours in each series of data are the real and imaginary components of the perturbation pressure of the wave $P(y, z)$ normalized according to conditions (2.56) and (2.57). We observe that for the range of α we have considered, the wave pressure shows relatively little variation.

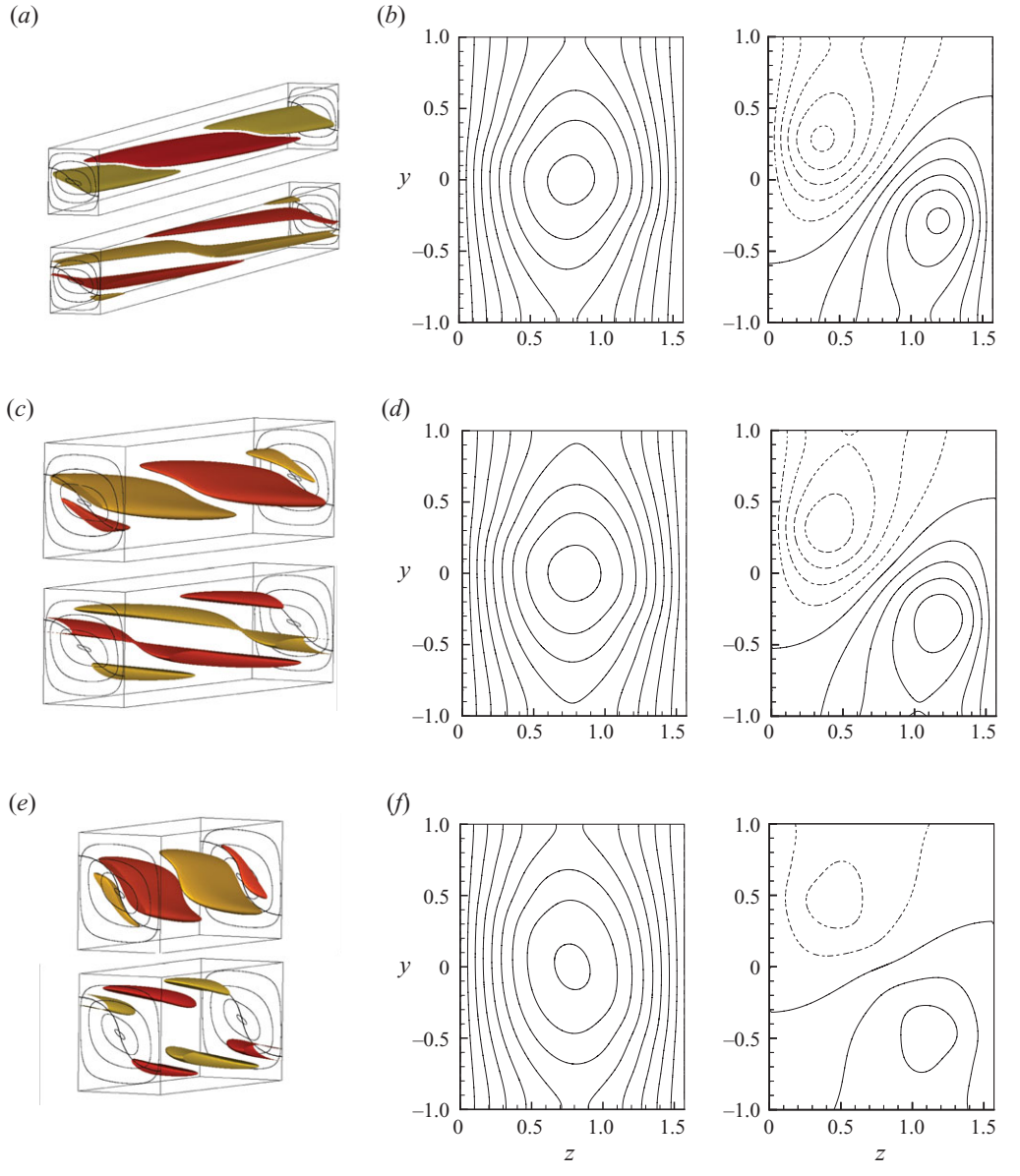

FIGURE 7. (Colour online) Wave field at three different axial wavelengths: $\alpha = 0.2$ (*a*,*b*), $\alpha = 0.8$ (*c*,*d*) and $\alpha = 1.4$ (*e*,*f*). The first column of images show the axial (*a*,*b*) and spanwise (*e*,*f*) wave components as isocontours (levels are at half the maximum and minimum values). The ends of these three-dimensional isocontours show the roll velocity and the critical layer by a solid bold line. The second and third columns of images show the real and imaginary perturbation pressure P fields. For the real fields, contours are plotted at equispaced levels of 0.2 intervals between 0 and 2. For the imaginary component, contours are plotted at equispaced levels of 0.1 intervals between -0.5 and 0.5. Dotted lines indicate negative contours. Pressure field is normalized according to conditions (2.56) and (2.57).

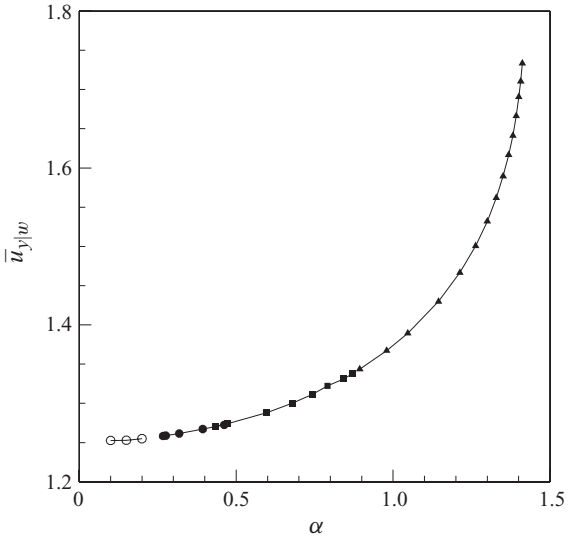

FIGURE 8. Variation of the mean wall shear rate $\bar{u}_{y|w}$ as a function of α evaluated for the values of ρ leading to $c=0$. The different symbols correspond to the search method adopted in obtaining data of figure 5.

Finally, in figure 8 we show the variation of the mean shear rate on the upper wall

$$\bar{u}_y|_{y=1} = \frac{1}{\Lambda}\int_{-\Lambda/2}^{\Lambda/2} \frac{\partial u}{\partial y}(1,z)\,\mathrm{d}z. \tag{4.1}$$

The shear rate determines the skin friction drag which will be induced by the streak system and is therefore of potential interest. We observe that for low values of α the non-dimensionalized shear rate has a minimum as α approaches 0. This figure is of considerable interest because there has been speculation that the lower branch states might be used as drag reduction devices by finding a control strategy to keep a turbulent flow close to these states. Hence, if that could be achieved at the optimum wavenumber shown, then the drag is about 25 % higher than the drag for Couette flow but much lower than the corresponding turbulent drag. The fact that the minimum drag occurs in the long wavelength limit is important and points to the importance of viscous effects which will come into play as the wavenumber decreases. In fact, it appears that the crucial limit is when αR is $O(1)$, in which case the wave evolves on the long length scale appropriate to the streak and in fact there is no decoupling between wave and vortex. This will be discussed subsequently.

Now let us now draw some conclusions from our work. We have shown that the lower branch states identified in Couette flow by a number of authors are closely related to vortex–wave interactions. The vortex–wave interaction theory is a high Reynolds theory whereas the lower branch states calculated by other authors correspond to numerical solutions of the full Navier–Stokes equations. The agreement we have found between the two approaches is excellent over a wide range of Reynolds numbers, and since the vortex–wave interaction theory reduces the computational problem from a three-dimensional Navier–Stokes problem to a two-dimensional steady Navier–Stokes problem, albeit with jump conditions to be imposed, coupled to a partial differential equation eigenvalue problem the vortex–wave approach might sensibly be used to generate solutions over a wide range of

parameters. Our formulation goes readily over to more general shear flows such as combined Couette–Poiseuille flow in a channel or Poiseuille flow in a pipe so the vortex–wave approach can be used for a variety of shear flows.

The relationship between self-sustained processes and vortex–wave interaction theories is in our opinion now clear. The vortex–wave interaction theories developed in a number of papers by Hall, Smith and coworkers provided a high Reynolds description of how finite amplitude wave systems which exist as instabilities of streaks can drive rolls that themselves drive the streaks. The mechanism is precisely the same as that subsequently used to describe self-sustained processes at finite Reynolds numbers. Here we have found that the lower branch Couette flow structures found by numerical solution of the Navier–Stokes equation are virtually identical to the vortex–wave interaction theory applied to inviscid waves over a wide range of Reynolds numbers. However, the self-sustained process approach has yielded upper branch solutions not described here, and it remains to be seen whether any of the other variants of vortex–wave interaction theory will lead to an asymptotic description of the upper branch modes. The key part of the interaction in both approaches is the process by which the waves feed energy back into the rolls. The alternative description of this provided in this paper is essentially a steady streaming approach and clearly reveals the details of this process. The first point to note is that the waves are inviscid and instantaneously neutral so that they will have a critical layer where the wave speed coincides with the streak velocity. In this layer the waves increase in amplitude and propagate predominantly in a thin viscous critical layer which is curved in the spanwise direction. The Reynolds stresses driven by the waves in this layer generate a mean normal pressure gradient and streaming velocity independent of time and the downstream variable. These lead to jumps in the normal derivative of roll velocity along the critical layer and the roll pressure. These effects drive the rolls and make the whole process sustainable.

One aspect of the lower branch states we have not addressed is their stability. Wang *et al.* (2007) numerically investigated the stability of these states and found that there was a single unstable eigenvalue which at large Reynolds numbers decayed approximately like $R^{-1/2}$. This was done by perturbing the Navier–Stokes equations about the lower branch solutions and solving numerically the resulting partial differential equation eigenvalue problem. This leads to one unstable eigenvalue with the Reynolds number dependence indicated above. A stability analysis of the equilibrium vortex–wave interaction equations is beyond the scope of this paper but some observations can be made.

Within our unsteady formulation of the vortex–wave interaction, the natural time scale for an instability of the combined wave–vortex state is R^{-1}. Therefore, if we perturb our equilibrium states within the framework of the unsteady interaction equations, then a linear instability analysis could be performed but the growth or decay rates of any disturbances are necessarily going to be of size R^{-1} so they could not describe the mode found by Wang *et al.* (2007). However, in different shear flows such modes might be unstable and play a role in the instability of lower branch modes. Therefore, the mode found by Wang *et al.* (2007) cannot be captured within the present framework. Professor Waleffe has kindly indicated that in his simulations of the instability the wave decays rapidly to zero, leaving a more slowly decaying streamwise vortex. Thus, the instability found by Wang *et al.* (2007) may well be a more rapidly growing secondary instability of the wave which leaves the vortex essentially undisturbed. If that is the case, the key would be to look for a more general critical layer structure allowing for the evolution of a wave on a faster time scale. This possibility is yet to be explored.

The authors would like to express their thanks to the referees for their many constructive comments on the original version of this paper and to Professor Fabian Waleffe for useful discussions regarding his work. The authors would also like to thank Dr B. Carmo for help with the calculations. S.J.S. would also like to acknowledge financial support under an EPSRC Advanced Research Fellowship.

REFERENCES

Ainsworth, M. & Sherwin, S. 1999 Domain decomposition preconditions for p and hp finite element approximation of Stokes equations. *Comp. Meth. Appl. Mech. Engng* **175**, 243–266.

Barkley, D., Blackburn, H. M. & Sherwin, S. J. 2008 Direct optimal growth analysis for timesteppers. *Intl J. Numer. Meth. Fluids* **57**, 1435–1450.

Bassom, A. & Hall, P. 1989 On the generation of mean flows by the interaction of Görtler vortices and Tollmien–Schlichting waves in curved channel flows. *Stud. Appl. Math.* **81**, 185–219.

Bennett, J., Hall, P. & Smith, F. 1991 The strong nonlinear interaction of Tollmien–Schlichting waves and Taylor–Görtler vortices in curved channel flow. *J. Fluid Mech.* **223**, 475–495.

Benney, D. 1984 The evolution of disturbances in shear flows at high Reynolds numbers. *Stud. Appl. Math.* **70**, 1–19.

Blackaby, N. 1991 On viscous, inviscid and centrifugal instability mechanisms in compressible boundary layers, including non-linear vortex/wave interactions and the effects of large Mach number on transition. PhD thesis, University of London.

Blackaby, N. & Hall, P. 1994 On the nonlinear secondary instability of a streamwise vortex flow. *Phil. Trans. Soc.* A **352**, 1700.

Brown, P., Brown, S., Smith, F. & Timoshin, S. 1993 On the starting process of strongly nonlinear vortex/Rayleigh-wave interactions. *Mathematika* **40** (1), 7–29.

Chapman, S. J. 2002 On the subcritical instability of channel flows. *J. Fluid Mech.* **451**, 35–97.

Clever, R. & Busse, F. 1997 Tertiary and quaternary solutions for plane Couette flow. *J. Fluid Mech.* **344**, 137–153.

Davey, A., DiPrima, R. & Stuart, J. 1968 On the instability of Taylor vortices. *J. Fluid Mech.* **31** (01), 17–52.

Faisst, H. & Eckhardt, B. 2003 Traveling waves in pipe flow. *Phys. Rev. Lett.* **91** (22), 224502.

Fitzgerald, R. 2004 New experiments set the scale for the onset of turbulence in pipe flow. *Phys. Today* **57** (2), 21–24.

Guermond, J. & Shen, J. 2003 Velocity-correction projection methods for incompressible flows. *SIAM J. Numer. Anal.* **41**, 112–134.

Hall, P. 1994 On the initial stages of vortex wave interactions in highly curved boundary layer flows. *Mathematika* **41** (1), 40–67.

Hall, P. & Horseman, N. 1991 The linear inviscid secondary instability of longitudinal vortex structures in boundary layers. *J. Fluid Mech.* **232**, 357–375.

Hall, P. & Morris, H. 1992 On the instability of boundary layers on heated flat plates. *J. Fluid Mech.* **245**, 367–400.

Hall, P. & Smith, F. 1988 The nonlinear interaction of Tollmien–Schlichting waves and Taylor–Görtler vortices in curved channel flows. *Proc. R. Soc. Lond.* A **417**, 255–282.

Hall, P. & Smith, F. 1989 Nonlinear a Tollmien–Schlichting/vortex interaction in boundary layers. *Eur. J. Mech.* B/*Fluids* **8** (3), 179–205.

Hall, P. & Smith, F. 1990 *Near Planar TS Waves and Longitudinal Vortices in Channel Flow: Nonlinear Interaction and Focussing*, pp. 5–39. Springer.

Hall, P. & Smith, F. 1991 On strongly nonlinear vortex/wave interactions in boundary-layer transition. *J. Fluid Mech.* **227**, 641–666.

Hof, B., van Doorne, C., Westerweel, J., Nieuwstadt, F., Faisst, H., Eckhardt, B., Wedin, H., Kerswell, R. & Waleffe, F. 2004 Experimental observation of nonlinear traveling waves in turbulent pipe flow. *Science* **305** (5690), 1594–1598.

Karniadakis, G. E., Israeli, M. & Orszag, S. A. 1991 High-order splitting methods for the incompressible Navier–Stokes equations. *J. Comput. Phys.* **97** (2), 414–443.

Karniadakis, G. E. & Sherwin, S. J. 2005 *Spectral/hp Element Methods for Computational Fluid Dynamics*, 2nd edn. Oxford University Press.

Kerswell, R. & Tutty, O. 2007 Recurrence of travelling waves in transitional pipe flow. *J. Fluid Mech.* **584**, 69–102.

LeTallec, P. & Patra, A. 1997 Non-overlapping domain decomposition methods for adaptive *hp* approximation of the Stokes problem with discontinuous pressure fields. *Comp. Meth. Appl. Mech. Engng* **145**, 361–379.

Li, F. & Malik, M. 1995 Fundamental and subharmonic secondary instabilities of Görtler vortices. *J. Fluid Mech.* **297**, 77–100.

Nagata, M. 1990 Three-dimensional finite-amplitude solutions in plane Couette flow: bifurcation from infinity. *J. Fluid Mech.* **217**, 519–527.

Riley, N. 1967 Oscillatory viscous flows: Review and extension. *J. Inst. Math. Appl.* **3**, 419–434.

Schneider, T., Gibson, J., Lagha, M., De Lillo, F. & Eckhardt, B. 2008 Laminar–turbulent boundary in plane Couette flow. *Phys. Rev.* E, 037301.

Stuart, J. T. 1966 Double boundary layers in oscillatory flow. *J. Fluid Mech.* **24**, 673–687.

Swearingen, J. & Blackwelder, R. 1987 The growth and breakdown of streamwise vortices in the presence of a wall. *J. Fluid Mech.* **182**, 255–290.

Taylor, G. 1923 Stability of a viscous liquid contained between two rotating cylinders. *Phil. Trans. R. Soc. Lond.* A **A223**, 289–343.

Timoshin, S. & Smith, F. 1997 Vortex/inflectional-wave interactions with weakly three-dimensional input. *J. Fluid Mech.* **348**, 247–294.

Tuckerman, L. S. & Barkley, D. 2000 Bifurcation analysis for timesteppers. In *Numerical Methods for Bifurcation Problems and Large-Scale Dynamical Systems* (ed. E. Doedel & L. S. Tuckerman), pp. 453–566. Springer.

Viswanath, D. 2007 Recurrent motions within plane Couette turbulence. *J. Fluid Mech.* **580**, 339–358.

Waleffe, F. 1995 Hydrodynamic stability and turbulence: beyond transients to a self-sustaining process. *Stud. Appl. Math.* **95** (3), 319–343.

Waleffe, F. 1997 On a self-sustaining process in shear flows. *Phys. Fluids* **9** (4), 883–900.

Waleffe, F. 1998 Three-dimensional coherent states in plane shear flows. *Phys. Rev. Lett.* **81** (19), 4140–4143.

Waleffe, F. 2001 Exact coherent structures in channel flow. *J. Fluid Mech.* **435**, 93–102.

Waleffe, F. 2003 Homotopy of exact coherent structures in plane shear flows. *Phys. Fluids* **15** (6), 1517–1534.

Walton, A. G. & Smith, F. 1992 Properties of strongly nonlinear vortex/Tollmien–Schlichting-wave interactions. *J. Fluid Mech.* **244**, 649–676.

Wang, J., Gibson, J. & Waleffe, F. 2007 Lower branch coherent states in shear flows: transition and control. *Phys. Rev. Lett.* **98** (20), 204501.

Wedin, H. & Kerswell, R. 2004 Exact coherent structures in pipe flow: travelling wave solutions. *J. Fluid Mech.* **508**, 333–371.

Yu, X. & Liu, J. 1991 The secondary instability in Goertler flow. *Phys. Fluids* **3** (8), 1845–1847.